TT20 Transport and Splitting of Beams Extracted Using Crystal Shadowing in LSS2 of the SPS

Pablo A. Arrutia Sota, Yann Dutheil, Matthew A. Fraser, Francesco M. Velotti

CERN, CH-1211 Geneva, Switzerland

Summary

The CERN Super Proton Synchrotron (SPS) is employed to supply slow extracted beams to fixed target experiments located in CERN's North Area. In order to reduce beam loss at extraction, several techniques have been proposed for implementation in the SPS. One of those techniques, which was tested with beam in 2018, uses a bent silicon crystal in Long Straight Section 2 (LSS2) to shadow the blade of the extraction electrostatic septum [7]. This approach alters the shape of the extracted particle distribution that needs to be transported and split in Transfer Tunnel 20 (TT20). This report studies the impact on the transmission and splitting efficiency with the crystal aligned in channelling and provides a solution for start-up after LS2 without hardware changes by modifying the transfer line optics. The main simulation code and files are available at https://gitlab.cern.ch/parrutia/beamlet_lss2.

Contents

1   Introduction

Transfer Tunnel 20 (TT20) connects the CERN Super Proton Synchrotron (SPS) with Target 2 (T2), Target 4 (T4) and Target 6 (T6) located in the CERN North Area (NA). A sketch of the TT20 layout with the naming conventions for all lines is provided in Figure 1 . Splitter 1 and Splitter 2 have identical geometries consisting of three Lambertson septa magnets (MSSB) in series and an upstream collimator (TCSC) that shields the magnets. This setup provides simultaneous beam to all targets. The cross-section geometry of the TCSC is provided in Figure 2.
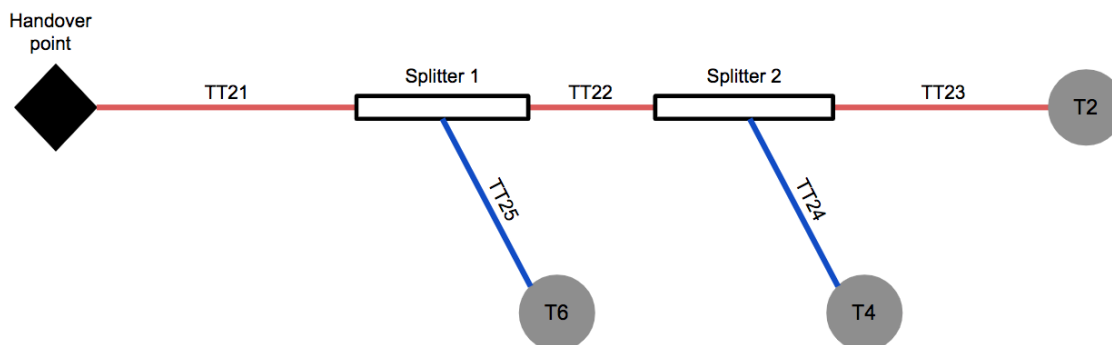

Figure 1: Layout of TT20 (not to scale). TT21 connects the Handover point with Splitter 1, which splits beam to TT22 and TT25. TT22 connects Splitter 1 with Splitter 2, which splits beam to TT23 and TT24.

As a mechanism to reduce beam loss during extraction, a silicon bent crystal has been installed in the SPS [7]. Silicon crystals have proven to be useful devices in deflecting highly energetic beams [6]. The crystal was installed immediately upstream of the extraction Electrostatic Septum (ZS) in Straight Section 216 of LSS2 to shadow the ZS by deflecting particles that would have otherwise impacted electrode wires. The maximum loss reduction expected and measured with the crystal in LSS2 is about 40% [7].

Consequently, the SPS will provide a different particle distribution to TT20, affected by the action of the crystal. It is important to asses the effects that this has on the particle losses along the transfer line and the distributions delivered to the targets. In this note we study these issues, identify possible aperture restrictions and provide a procedure to minimise undesired losses by adjusting TT20 optics.

2   Beam Characterisation

This section briefly characterises the beam profile that will result from the crystal-aided extraction and compares it to the profile without a crystal.

The profile without a crystal and its setup are referred to as the *nominal beam* and the *nominal setup*, respectively. It will be shown that the new distribution calls for a study of aperture constraints and loss optimisation in TT20.
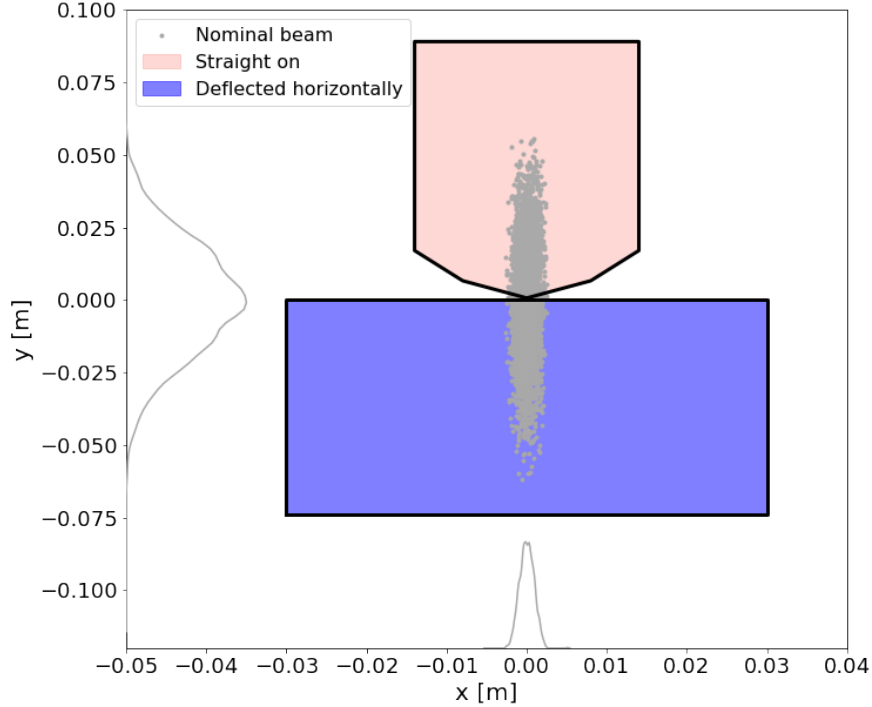
Figure 2: Front face of TCSC. Particles that enter the top hole continue straight towards TT22 (Splitter 1) or TT23 (Splitter 2). Particles that enter the bottom hole are horizontally deflected towards TT25 (Splitter 1) or TT24 (Splitter 2). Particles that hit the blade are lost.

In Figure 3, the beam distribution with the crystal aligned in channelling is shown at the handover point, which is located downstream of QDA219. It can be characterised as follows:

1. In the horizontal phase space, the beam with crystal-shadowing is identical to the nominal one but with an added beamlet, as shown in Figure 3a. In other words, the crystal array does not perturb the nominal beam being extracted, but allows to extract an extra patch of particles by horizontally kicking them away from the ZS wires. Throughout the note, the term *core* refers to solely the unperturbed part of the beam, the term *beamlet* to the particles that result from the interaction with the crystal, and the term *beam* to the union of both the core and the beamlet.

2. In vertical phase space, the beam remains practically identical to the nominal case as shown in Figure 3b, as the crystal has no action in the vertical plane (other than negligible scattering effects).

3. The beamlet intensity $I_{beamlet}$ comprises a small part of the total beam intensity I_{beam}. In our simulations we take $I_{beamlet} \approx 1.8\% \cdot I_{beam}$, which is in close agreement with the increase in extracted intensity of 1.5% measured in [4].

Item 2 ensures that the beamlet will not pose any extra aperture constraints in the vertical plane through TT20. However, Item 1 calls for a closer inspection of the horizontal

4

(a) Horizontal phase space.
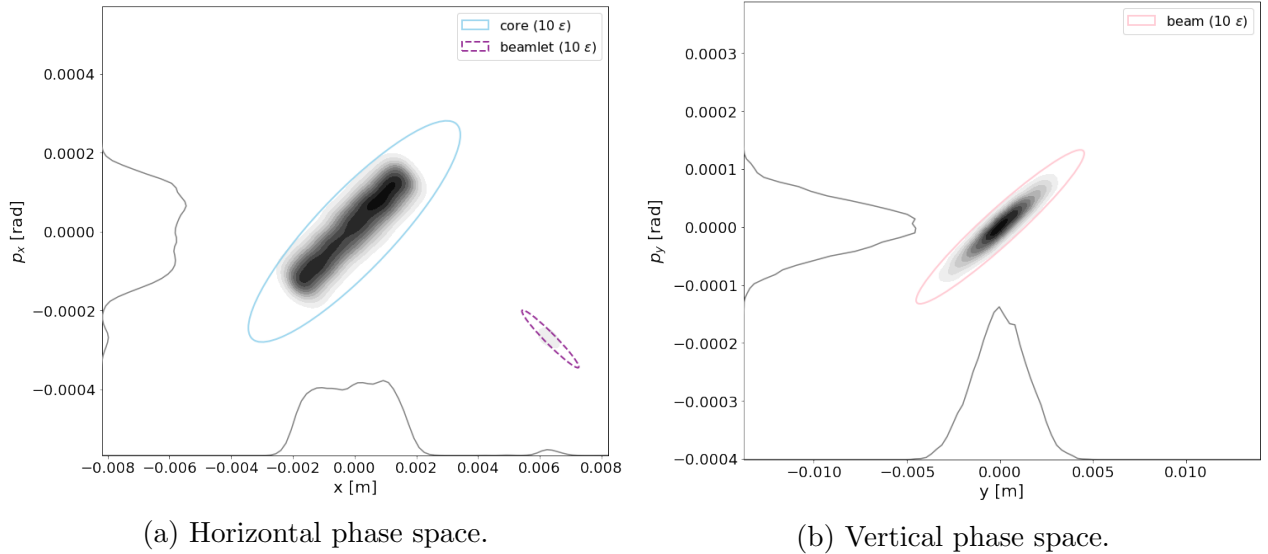
(b) Vertical phase space.

Figure 3: Beam phase-space at the handover point in the presence of the crystal shadowing the ZS and aligned in channelling.

propagation of the new beam, as the beamlet has a large horizontal amplitude (around 17.5σ) compared to the core. This is also completely in agreement with what was observed during the data taking documented in [7]. Furthermore, Item 3 indicates that losing the beamlet in an undesired location could lead to a localised region of radioactivation (a hotspot) or even damage.

3   Beam Propagation Down TT21

In order to propagate the beam down TT21, Courant-Snyder beam parameters were separately estimated for both the core and the beamlet at the Handover point. They are listed in Table 1 and their corresponding ellipses are shown in Figure 3.

Throughout this note, this parametric representation of the beam is used to provide an intuition of aperture constraints, but particle tracking via MADX-PTC [3] is in fact used to compute numerical values for beam loss processes. Figures 4 and 5 show the horizontal and vertical beam sizes under the nominal optics along TT21, which connects the handover point with the entrance of Splitter 1. It can be seen that the large horizontal excursions of the beamlet result in new aperture limitations. A detailed description of the optics applied in TT20 can be found in Appendix A.

4   Possible Solutions

Broadly speaking, we can define a possible solution as a modification of the nominal setup that (i) avoids a significant increase in losses compared to the nominal beam, specially in unwanted locations (dipoles, quadrupoles...) and (ii) provides usable beam to all targets.

Table 1: RMS parameters at the handover point. The chosen normalised emittances $\epsilon_{x,N}^{upper}$ and $\epsilon_{y,N}^{upper}$ are upper bounds on the values that can be observed from SPS extractions.

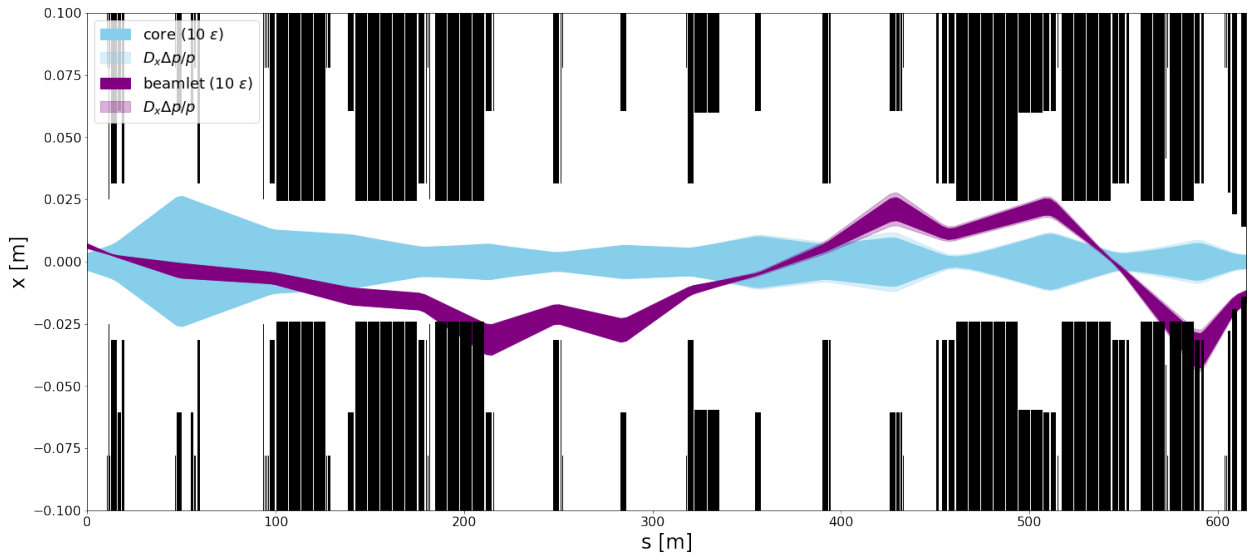|	Core	Beamlet
β_x [m]	24.99	48.69
α_x [rad]	-1.78	3.73
D_x [m]	0.01	-0.01
D_{px} [mrad]	1.26	0.60
x [m]	-0.00	0.01
p_x [mrad]	0.00	-0.27
β_y [m]	113.54	112.11
α_y [rad]	-3.19	-3.12
D_y [m]	-0.03	0.00
D_{py} [mrad]	-0.92	0.44
y [m]	0.00	0.00
p_y [mrad]	0.00	0.00
$\epsilon_{x,N}^{upper}$ [mm mrad]	20.10	0.74
$\epsilon_{y,N}^{upper}$ [mm mrad]	7.65	7.92

Figure 4: TT21 horizontal transport with nominal setup. The lighter envelopes indicate the increased beam size due to $\Delta p/p = \pm 1.5e - 3$. The beamlet is highly constrained in two locations: $s \approx 200$ m and $s \approx 580$ m.

The transmission and splitting efficiency can be formalised quite concretely as an optimisation problem, where one tries to minimise the total losses in the transfer line by allowing certain knobs to be varied from their nominal values. This was the approach pursued to find all the solutions listed in this note. Particularly, the loss function $\overline{L}$ to be minimised was chosen to be,

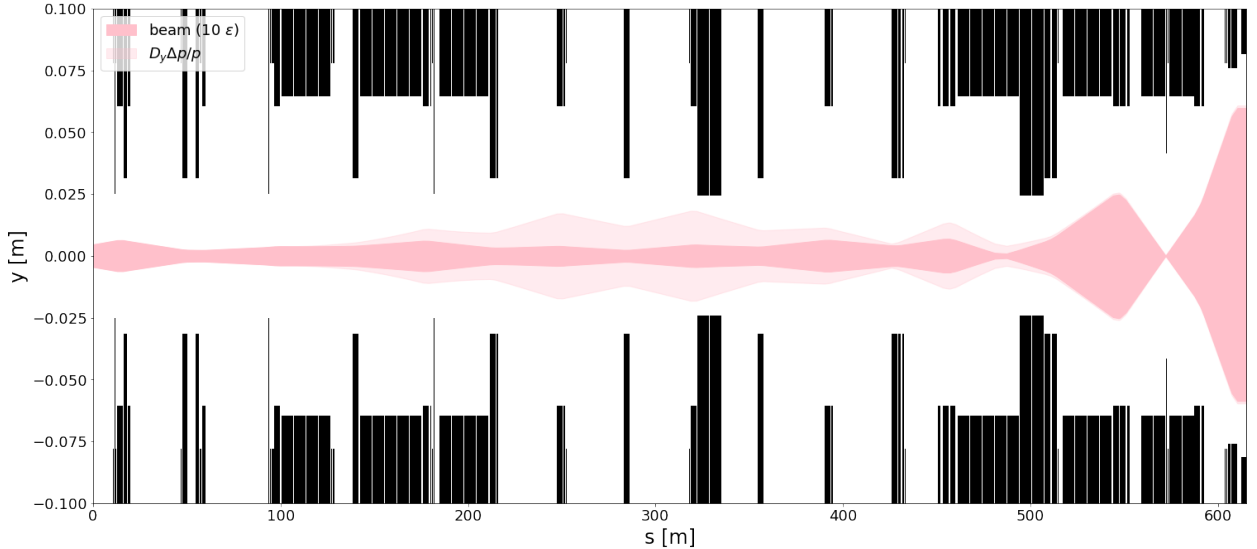$$\overline{L} = l_{split} + 100 \cdot l_{elsewhere}, \tag{1}$$

6

Figure 5: TT21 vertical propagation with nominal setup. The lighter envelopes reflect the increased beam size due to $\Delta p/p = \pm 1.5e-3$.

where l_{split} are the losses in the splitting regions and $l_{elsewhere}$ are the losses anywhere else. $l_{elsewhere}$ is heavily weighted to emphasise losses in undesired locations - the particular value of 100 was empirically chosen.

Optimisation of the beam distributions at the targets is not formalised neither inspected in detail. However, we assume that deviating as little as possible from the distributions delivered by the nominal setup is a positive quality of any modification. One could imagine enforcing such a quality by adding a term in the loss function that depends on some or all RMS beam parameters at the targets.

In the following subsections specific possible solutions are provided, focusing on those that could immediately be implemented after CERN's Long Shutdown 2. Other solutions that would require hardware modifications, *e.g.* the installation of a dedicated collimator to absorb the beamlet, or emittance exchange to rotate the beamlet into the vertical plane are not discussed here and are being investigated in the scope of future conceptual design studies [2].

4.1 Horizontal Steering Only

It is possible to horizontally steer the beam such that aperture constraints are overcome, as shown in Figure 6. A simple implementation would consist in minimising the losses in TT20 by varying only the horizontal correctors in TT21, subject to their respective strength constraints. In this case, $\overline{L}$ was minimised employing the Nelder-Mead algorithm [5]. The correctors' names and their respective strengths are listed in Appendix C, Table 5.

When the beam does not need to be split, this routine provides a valid solution. For example, and albeit with a different TT20 optics, this could be done for the future SPS-BDF [1] beam in presence of a beamlet, as shown already in measurements [7]. However, for beams that need to be split, the obtained setup increases losses on Splitter 1 by a factor 2
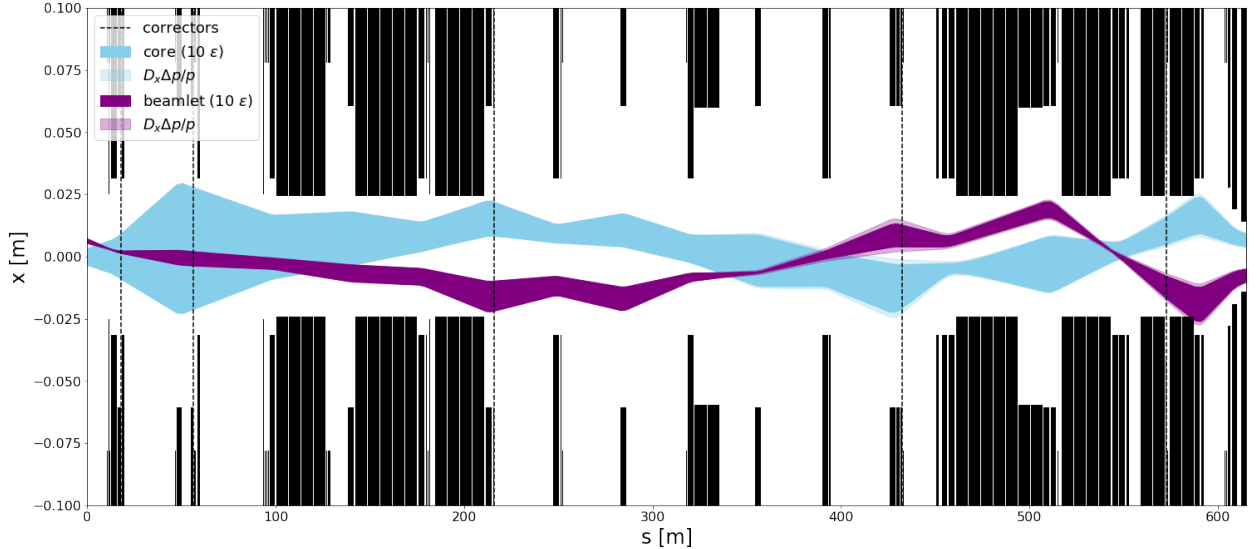
Figure 6: TT21 horizontal propagation with correctors to minimise losses.

with respect to the nominal setup. This is mainly due to two reasons:

- Losses at the splitters are very sensitive to horizontal misalignments in both position and angle because of the vertical slope of the hole's geometry in the magnet's yoke. As a reference, Figure 7 shows the losses of the nominal beam on Splitter 1 alone when misalignments are introduced.

- There are no horizontal correctors after the last main aperture constraint in TT21 ($s \approx 580$ m), which means misalignments will be present in Splitter 1.

4.2   Horizontal Steering and Varying Quadrupole Strengths

In the same spirit as the previous section, one could allow quadrupole strengths to vary, as well as corrector strengths. The problem starts to have more degrees of freedom, but the same ideas apply. It is important to point out that the beam loss is sensitive to the horizontal beam size due to the vertical slope on the splitter hole.

In principle, one could allow all quadrupole and corrector strengths to vary, essentially asking the optimization problem to entirely redesign the optics of TT20 with the sole purpose of minimizing losses. In our particular problem, this seems like an overly complicated and counterproductive task and especially difficult to constrain with algorithm applied in operation. Therefore, we opt for a minimal approach that departs as little as possible from the nominal setup:

1. A closed bump like the one shown in Figure 8 is created to avoid the first aperture restriction. Appropriate horizontal corrector strengths were found with the aid of MADX's matching command. The correctors' names and their respective strengths are listed in Appendix C, Table 6.

8

2. Only quadrupole strength *k2114m* is included in the minimisation routine. *k2114m* controls the focusing quadrupole family upstream of the last aperture constraint, ensuring optics remain unchanged for as far down the line as possible.

3. A local optimiser is chosen to limit exploration. In particular, the Nelder-Mead algorithm showed satisfactory performance in solving the problem without perturbing optics significantly.
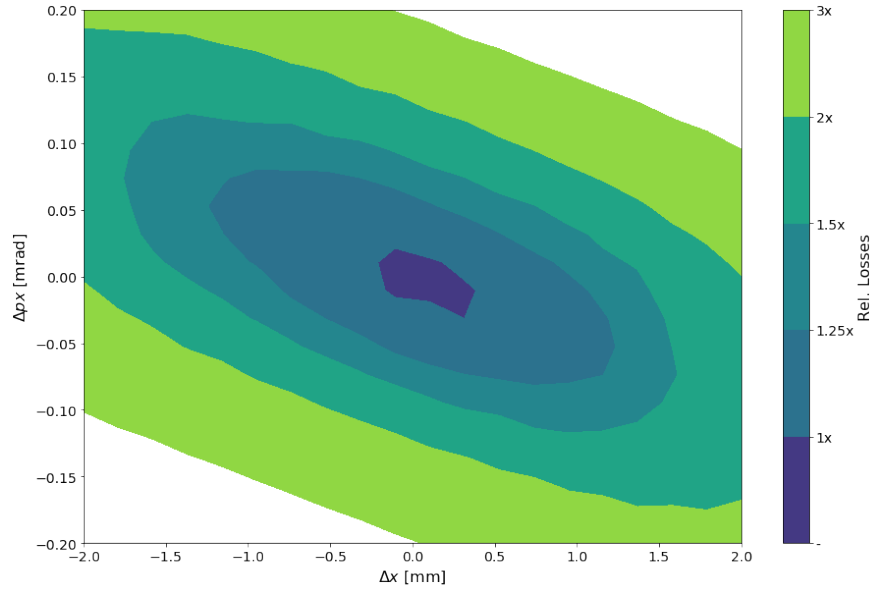

Figure 7: Heatmap of the relative increase in losses of the nominal beam when misalignments are introduced at Splitter 1.
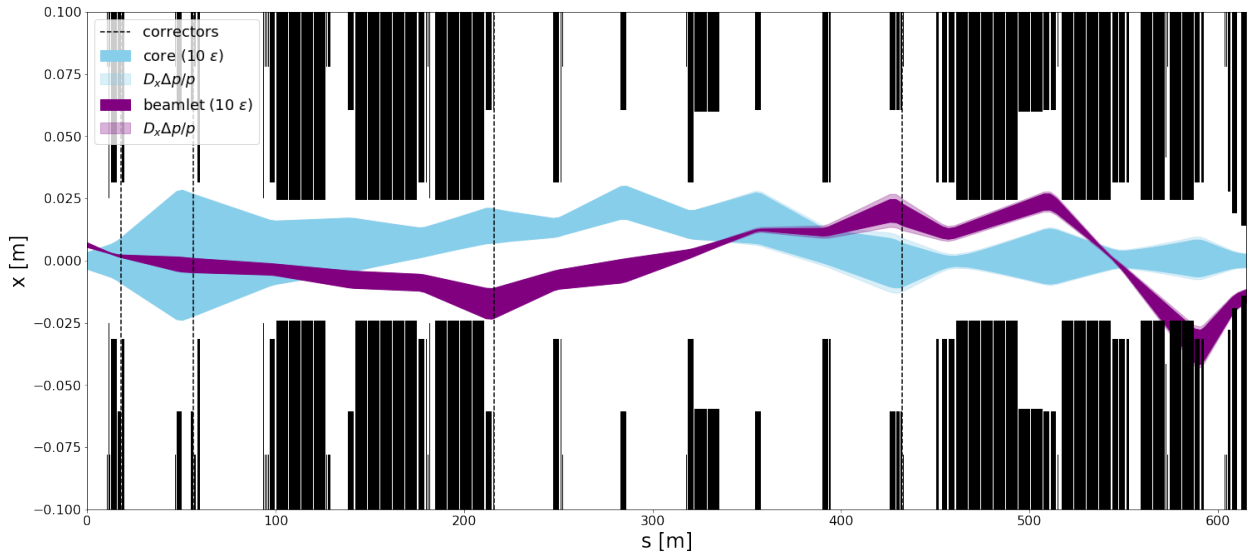

Figure 8: TT21 horizontal propagation with a closed bump. The beam avoids the first aperture restriction.

9

The propagation of the beam under the found setup can be seen in Figure 9. The setup produces an 18% increase in losses at the splitters and fully avoids losses elsewhere. The relative change in quadrupole strengths and the variation in β functions can be seen in Figure 10.
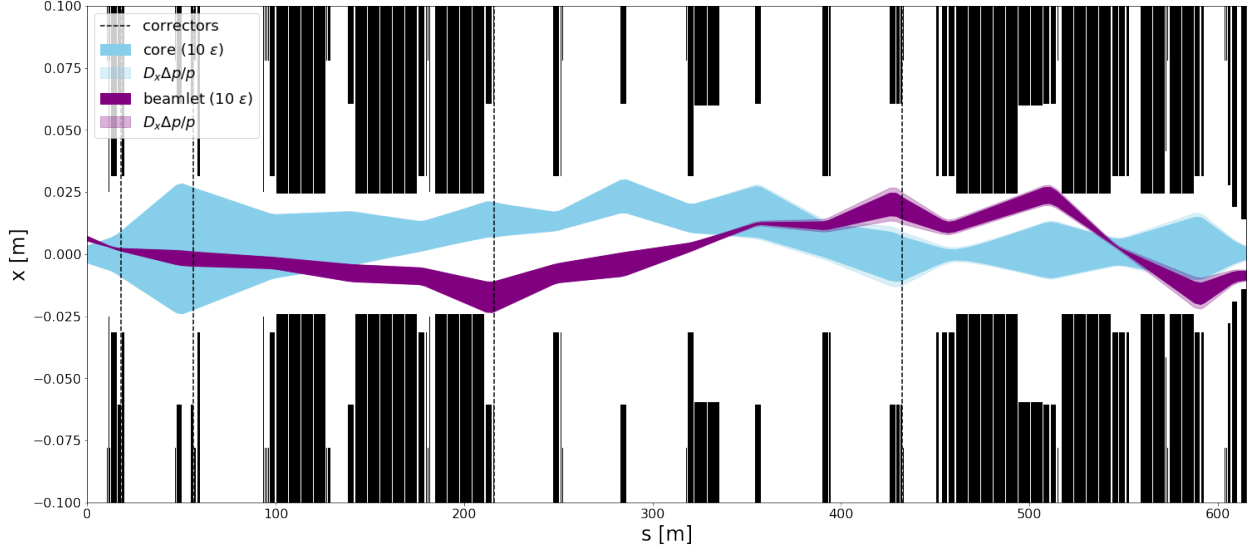
Figure 9: TT21 horizontal propagation with optimised k2114m strength. The beam avoids both aperture restrictions.
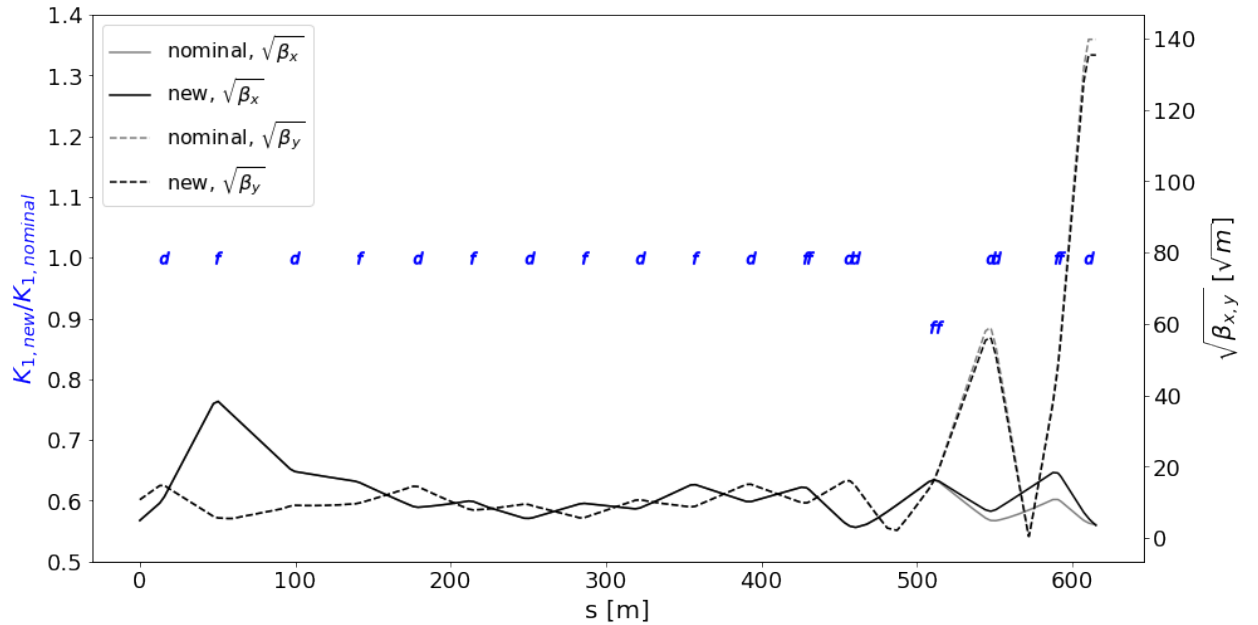
Figure 10: Relative changes in quadrupole strengths and β functions along TT21 with optimised k2114m strength. $\sqrt{\beta_{x,y}}$ is plotted to show the relative change in beam size. The f-shaped and d-shaped markers denote focusing and defocusing quadrupoles, respectively.

The changes perturb the phase space parameters of the beam at the targets. The beam

profiles at T2, T4 and T6 can be seen in Figures 11, 12, 13, respectively. The RMS parameters are listed in Appendix B. The change in parameters is visible, but small. It is reasonable to assume that rematching the optics upstream of the targets would reduce this difference, if needed.


(a) Horizontal phase space.

(b) Vertical phase space.

Figure 11: New beam profile at T2. The parametric ellipse of the nominal setup is also shown for comparison.

(a) Horizontal phase space.

(b) Vertical phase space.

Figure 12: New beam profile at T4. The parametric ellipse of the nominal setup is also shown for comparison.

It is important to mention that one could gradually increase the degrees of freedom of the setup, seeking an even larger reduction in losses at the cost of adding complexity and deviating from the nominal setup.
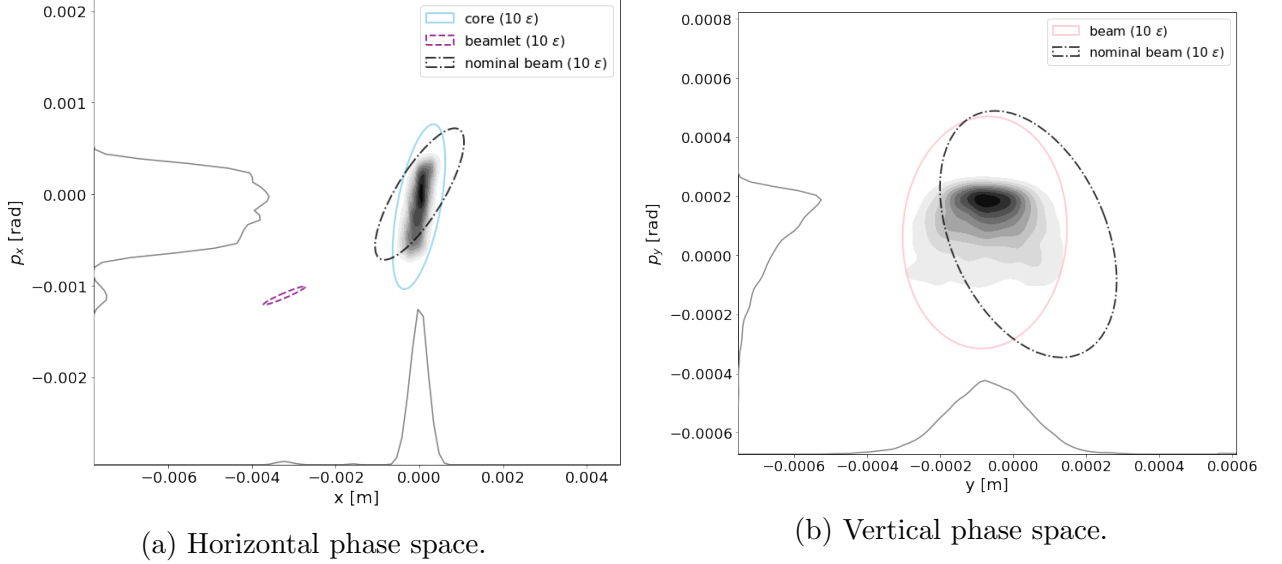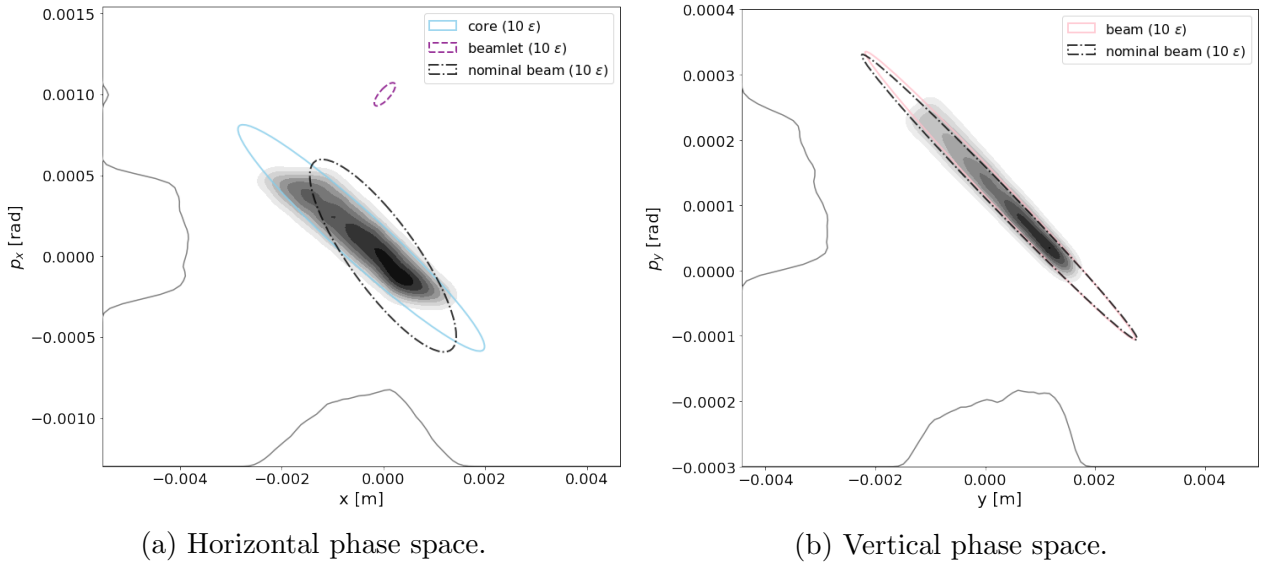
(a) Horizontal phase space.
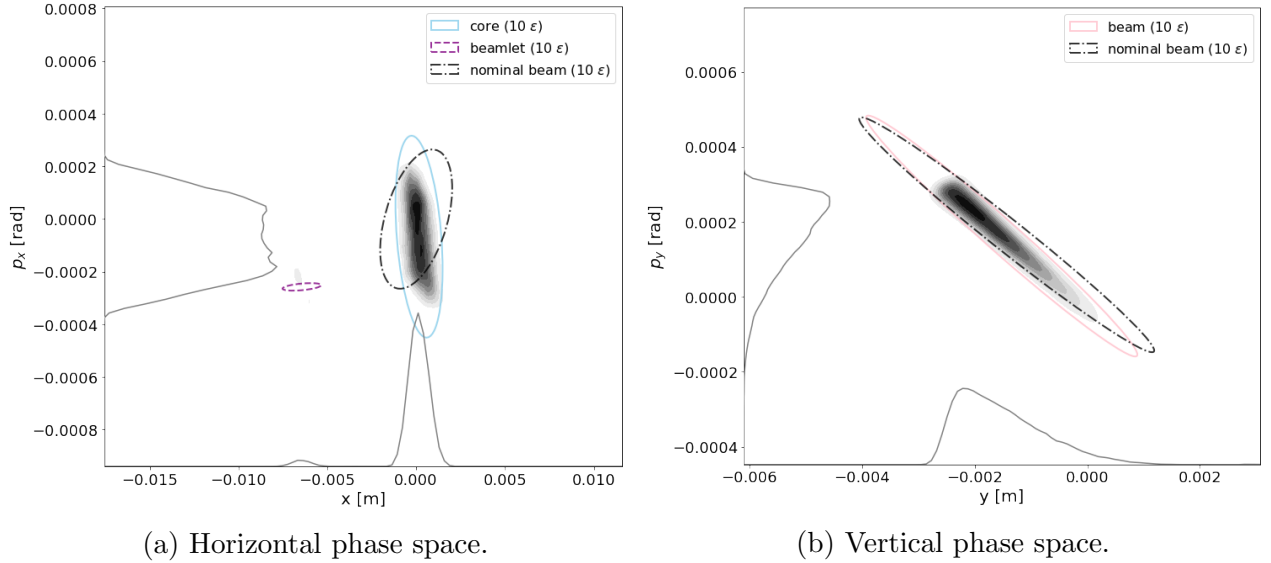
(b) Vertical phase space.

Figure 13: New beam profile at T6. The parametric ellipse of the nominal setup is also shown for comparison.

Further studies will be carried out to implement this optimisation procedure in operation.

5 Conclusion

The thin, bent crystal installed in LSS2 of the SPS will add a beamlet to the distribution that needs to be transported down TT20 as it oscillates around the beam's core. The beamlet introduces new aperture constraints that need to be addressed. By combining both correctors and quadrupoles, a conceptual solution with only an 18% increase in beam loss at Splitter 1 was found, whilst the beam loss in the SPS is reduced by over 40%. This compares to a horizontal misalignment at the splitter of a millimeter. The procedure involves minimising our chosen penalty function, $\overline{L}$ (See Equation 1), by varying magnet strengths. An operational implementation of the optimiser should be feasible by trimming a closed-orbit correction and a single power converter whilst acquiring beam loss signals. The proposed solution in this note could be immediately implemented after Long Shutdown 2.

A   Optics

The optics considered as nominal in this note are shown in Figures 14 and 15. Table A lists the main optical parameters at key locations, namely the Handover point, the position monitors and the front face of Splitter 1.
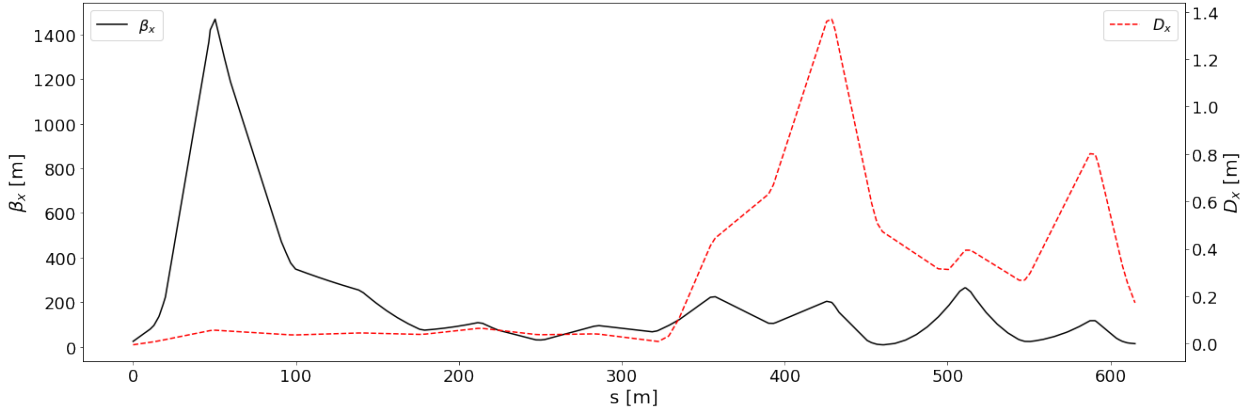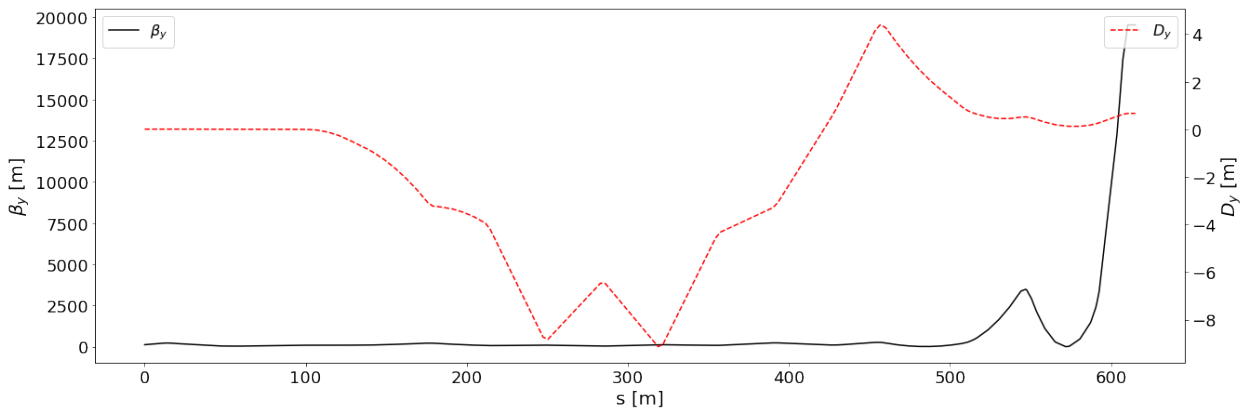

Figure 14: TT21 nominal horizontal optics

Figure 15: TT21 nominal vertical optics

	s	β_x	β_y	D_x	D_y	μ_x	μ_y
ejpt	0.00	24.62	116.30	-0.00	0.01	0.00	0.00
bsg.210023	11.00	83.09	200.56	0.01	0.01	0.04	0.01
bbs.210025	11.70	88.16	206.75	0.01	0.01	0.04	0.01
btv.210026	12.40	93.40	213.04	0.01	0.01	0.04	0.01
bsg.210156	46.95	1394.42	38.40	0.05	0.00	0.06	0.07
bsp.210215	57.19	1262.23	30.41	0.05	0.00	0.06	0.12
bsi.210216	57.89	1241.97	30.41	0.05	0.00	0.06	0.12
bbs.210276	93.81	423.34	73.62	0.04	-0.00	0.07	0.26
bsi.210278	94.74	407.97	75.85	0.04	-0.00	0.07	0.26
bsi.210279	95.62	393.57	78.04	0.04	-0.00	0.07	0.27
bsg.210350	127.50	278.89	86.80	0.04	-0.47	0.08	0.33
btv.210352	128.90	275.70	87.41	0.04	-0.52	0.08	0.33
bsp.210508	181.31	76.36	194.84	0.04	-3.25	0.14	0.39
bbs.210509	182.01	76.80	190.92	0.04	-3.25	0.15	0.39
bsp.210858	318.32	67.69	110.99	0.01	-9.10	0.49	0.73
bsi.211626	604.12	36.94	13365.24	0.42	0.55	1.25	1.88
btv.211628	604.82	34.01	14192.45	0.40	0.57	1.26	1.88
splitter1.up	612.46	16.11	19522.34	0.22	0.67	1.31	1.88

B   RMS Parameters at Targets

The RMS parameters for the distributions at the targets are listed here. The ellipses in Figures 11, 12 and 13 have been drawn based on tables 2, 3 and 4, respectively.

Table 2: RMS parameters at T2.

	Core	Beamlet	Nominal Beam
β_x [m]	0.84	17.11	2.43
α_x [rad]	-0.67	-3.31	-1.31
D_x [m]	0.04	0.07	0.00
D_{px} [mrad]	-40.69	-65.78	-40.53
x [m]	-0.00	-0.00	0.00
p_x [mrad]	-0.14	-1.11	0.00
$\epsilon_{x,N}$ [mm mrad]	19.97	0.62	19.77
β_y [m]	0.58	0.67	0.62
α_y [rad]	-0.05	-0.01	0.39
D_y [m]	0.10	0.15	0.07
D_{py} [mrad]	-7.17	-15.92	-4.72
y [m]	-0.00	-0.00	0.00
p_y [mrad]	0.08	-0.01	0.07
$\epsilon_{y,N}$ [mm mrad]	3.78	2.63	3.99

Table 3: RMS parameters at T4.

	Core	Beamlet	Nominal Beam
β_x [m]	12.35	4.48	4.36
α_x [rad]	3.43	-1.18	1.51
D_x [m]	-0.42	-0.65	-0.38
D_{px} [mrad]	14.68	9.79	15.85
x [m]	-0.00	0.00	-0.00
p_x [mrad]	0.11	1.00	0.00
$\epsilon_{x,N}$ [mm mrad]	20.29	0.41	20.16
β_y [m]	98.90	80.18	104.56
α_y [rad]	8.80	7.55	9.05
D_y [m]	-0.11	0.01	-0.08
D_{py} [mrad]	-5.62	-20.86	-5.01
y [m]	0.00	-0.00	0.00
p_y [mrad]	0.12	0.16	0.11
$\epsilon_{y,N}$ [mm mrad]	2.63	1.38	2.58

Table 4: RMS parameters at T6.

	Core	Beamlet	Nominal Beam
β_x [m]	3.64	85.85	8.58
α_x [rad]	0.34	-0.52	-0.50
D_x [m]	0.37	0.39	0.29
D_{px} [mrad]	-49.09	-59.45	-47.44
x [m]	0.00	-0.01	0.00
p_x [mrad]	-0.07	-0.26	0.00
$\epsilon_{x,N}$ [mm mrad]	20.45	0.59	20.33
β_y [m]	41.85	41.04	48.59
α_y [rad]	5.50	5.35	5.73
D_y [m]	-0.07	-0.04	-0.04
D_{py} [mrad]	0.60	-3.84	3.45
y [m]	-0.00	-0.00	-0.00
p_y [mrad]	0.16	0.16	0.17
$\epsilon_{y,N}$ [mm mrad]	5.88	6.08	5.99

C   Corrector Strengths

The corrector strengths for the discussed setups are listed here.

C.1   Horizontal Steering Only

The horizontal steering setup uses the correctors and corrector strengths listed in Table 5.

Table 5: Angular kicks and their limits at $p_0 = 400 GeV/c$ for horizontal steering setup.

	$k_0 L$ [**rad**]	$|k_{0,max/min}|L$ [**rad**]
mdlh.210106	1.0e-4	1e-3
mdlh.210212	1.6e-5	1e-3
mdsh.210606	-2.5e-5	6e-4
mdsh.211209	2.1e-5	6e-4
mpls.211546	6.5e-5	5e-5

C.2   Closed Bump

The closed bump setup uses the correctors and corrector strengths listed in Table 6.

Table 6: Angular kicks and their limits at $p_0 = 400 GeV/c$ for closed bump setup.

	$k_0 L$ [**rad**]	$|k_{0,max/min}|L$ [**rad**]
mdlh.210106	6.6e-5	1e-3
mdlh.210212	2.4e-5	1e-3
mdsh.210606	1.2e-4	6e-4
mdsh.211209	2.0e-4	6e-4

References

[1] Claudia Christina Ahdida, Gianluigi Arduini, Michele Battistin, Markus Brugger, Marco Calviani, Brennan Goddard, Richard Jacobsson, Mike Lamont, Jeremie Bauche, Mirko-antonio Casolino, N. Colonna, Liam Andrew Dougherty, Yann Dutheil, Matthew Alexander Fraser, Lau Gatignon, Jonathan Gall, Simone Gilardoni, Jean-Louis Grenard, Damien Grenier, Verena Kain, Keith Kershaw, Eirini Koukovini Platia, Edmundo Lopez Sola, Simon Marsh, Richard Francis Morton, Yvon Muttoni, John Andrew Osborne, Pierre Ninin, Antonio Perillo Marcone, Francisco Sanchez Galan, Pablo Santos Diaz, Sabrina Schadegg, Linda Stoel, Claudio Leopoldo Torregrosa Martin, Heinz Vincke, Helmut Vincke, Francesco Maria Velotti, Thijs Wijnands, and Owain Edwyn Williams. *SPS Beam Dump Facility - Comprehensive Design Study*. CERN Yellow Reports: Monographs. Dec 2019.

[2] Pablo Andreas Arrutia Sota. Loss reduction techniques for slow extraction and beam delivery from synchrotrons. Unpublished masters thesis, 2020.

[3] Laurent Deniau, Hans Grote, Ghislain Roy, Frank Schmidt, Iselin F.C., W. Herr, and many other contributers. MADX. http://mad.web.cern.ch/mad/.

[4] M. Fraser, L.S. Esposito, F. Galluccio, Y. Gavrikov, B. Goddard, V. Kain, M. Pari, J.P Prieto, R. Rossi, W. Scandale, L.S. Stoel, and F.M. Velotti. Results from test of tecs in sps lss2 during operation in vr. In *SLAWG-CASE WG Meeting*, page 11, 2018.

[5] F. Gao and L. Han. Implementing the nelder-mead simplex algorithm with adaptive parameters. *Comput Optim Appl*, 51:259 – 277, 2012.

[6] W. Scandale, R. Losito, M. Silari, E. Bagli, S. Baricordi, P. Dalpiaz, M. Fiorini, V. Guidi, A. Mazzolari, D. Vincenzi, R. Milan, Gianantonio [Della Mea], E. Vallazza, A.G. Afonin, Yu.A. Chesnokov, V.A. Maisheev, I.A. Yazynin, S.V. Afanasiev, A.D. Kovalenko, A.M. Taratin, V.V. Uzhinsky, A.S. Denisov, Yu.A. Gavrikov, Yu.M. Ivanov, L.P. Lapina, L.G. Malyarenko, V.V. Skorobogatov, V.M. Suvorov, S.A. Vavilov, D. Bolognini, S. Hasan, and M. Prest. Probability of inelastic nuclear interactions of high-energy protons in a bent crystal. *Nuclear Instruments and Methods in Physics Research Section B: Beam Interactions with Materials and Atoms*, 268(17):2655 – 2659, 2010.

[7] Francesco Maria Velotti, Luigi Salvatore Esposito, Matthew Alexander Fraser, Verena Kain, Simone Gilardoni, Brennan Goddard, Michelangelo Pari, Javier Prieto, Roberto Rossi, Walter Scandale, Linda Susan Stoel, Francesca Galluccio, Marco Garattini, and Yury Gavrikov. Septum shadowing by means of a bent crystal to reduce slow extraction beam loss. *Phys. Rev. Accel. Beams*, 22:093502, Sep 2019.